FUDMA Journal of Sciences (FJS)
ISSN online: 2616-1370
ISSN print: 2645 - 2944
Vol. 10 No. 17, September, 2026, pp 9 – 25
DOI: https://doi.org/10.33003/fjs-2026-1017-5904

Click Chemistry-Mediated Synthesis, Spectroscopic Characterization, and Antimicrobial Evaluation of a Benzyl-Substituted 1,2,3-Triazole

[1]Grema A. Mala, [1]Ibrahim M. Wakil, [1]Abubakar A. Ahmeda, [2]Hauwa A. Zarma, [1]Hassan I. Musa and *[1,3]Ibrahim Waziri

[1]Department of Pure and Applied Chemistry, University of Maiduguri, P.M.B. 1069, Maiduguri, Nigeria.
[2]Department of Nutrition and Dietetics, University of Maiduguri, P.M.B. 1069, Maiduguri, Nigeria.
[3]Department of Chemical Science, University of Johannesburg, P.O. Box 524, Auckland Park Kingsway 2006, Johannesburg, South Africa.

*Corresponding authors' email: triumph2236@gmail.com

Received: 12 May 2026
Accepted: 25 May 2026
Published: 18 May 2026

ABSTRACT

The increasing prevalence of antimicrobial resistance has intensified the search for new heterocyclic scaffolds with improved biological activity. In this study, a novel 1,2,3-triazole derivative, 1-benzyl-4-((4-nitrophenoxy)methyl)-1*H*-1,2,3-triazole (PNT), was synthesized via a copper(I)-catalyzed azide–alkyne cycloaddition (CuAAC) reaction and characterized using Fourier-transform infrared spectroscopy (FTIR), ultraviolet-visible (UV–Vis) spectroscopy, ^{1}H and ^{13}C nuclear magnetic resonance (NMR) spectroscopy, and high-resolution mass spectrometry (HRMS). The antimicrobial potential of PNT was evaluated against six bacterial (*Staphylococcus aureus*, *Streptococcus pyogenes*, *Streptococcus faecalis*, *Escherichia coli*, *Salmonella typhi*, and *Klebsiella pneumoniae*) and two fungal (*Candida albicans* and *Aspergillus fumigatus*) strains using the agar well diffusion method, followed by determination of the minimum inhibitory concentration (MIC), minimum bactericidal concentration (MBC), and minimum fungicidal concentration (MFC). The compound exhibited concentration-dependent antimicrobial activity, with the largest inhibition zone observed against *Klebsiella pneumoniae* (18.00 ± 0.26 mm at 100 µg/mL), while *Aspergillus fumigatus* was the most susceptible fungal isolate (17.00 ± 0.56 mm). MIC/MBC values of 1.56 µg/mL were obtained against *Staphylococcus aureus*, whereas MIC/MFC values of 1.56 µg/mL were recorded for *Aspergillus fumigatus*, indicating bactericidal and fungicidal activities at the inhibitory concentration. Activity index analysis further demonstrated appreciable relative antimicrobial efficacy, with values of 44.0% and 43.5% against *Aspergillus fumigatus* and *Staphylococcus aureus*, respectively. The observed antimicrobial activity is attributed to the synergistic contribution of the 1,2,3-triazole nucleus, benzyl substituent, and electron-withdrawing nitrophenoxy moiety, which collectively provide a promising pharmacophoric framework. These findings identify PNT as a promising lead compound for the development of new triazole-based antimicrobial agents and warrant further structural optimization and mechanistic investigations.

Keywords: 1,2,3-Triazole, Click Chemistry, Antimicrobial Activity, Minimum Inhibitory Concentration, Activity Index, Heterocyclic Compounds

INTRODUCTION

The rapid emergence and global dissemination of antimicrobial resistance (AMR) have become major public health concerns, substantially diminishing the effectiveness of existing antibacterial and antifungal therapies (Ahmad *et al.*, 2026; Ahmed *et al.*, 2024). This escalating crisis has intensified efforts toward the discovery of structurally diverse antimicrobial agents possessing novel mechanisms of action capable of overcoming current resistance pathways (Ibisanmi *et al.*, 2026; Lucero-Prisno III *et al.*, 2025). Among the numerous heterocyclic scaffolds explored in medicinal chemistry, 1,2,3-triazoles have attracted considerable attention owing to their exceptional chemical stability, synthetic accessibility, and diverse pharmacological properties, including antibacterial, antifungal, antiviral, anticancer, anti-inflammatory, and antitubercular activities (Bozorov *et al.*, 2019; Dar *et al.*, 2025; Dixit *et al.*, 2021).

The development of copper(I)-catalyzed azide–alkyne cycloaddition (CuAAC), widely known as *click chemistry*, has revolutionized the synthesis of 1,2,3-triazole derivatives by providing a highly efficient, regioselective, and modular synthetic strategy (Campana *et al.*, 2026; Vala *et al.*, 2026). This transformation proceeds under mild reaction conditions with excellent functional-group tolerance and consistently affords thermodynamically stable 1,4-disubstituted 1,2,3-triazoles in high yields. Consequently, CuAAC has become one of the most powerful synthetic methodologies for constructing molecular libraries and developing biologically active compounds with tailored physicochemical and pharmacological properties (El Malah *et al.*, 2020; Singh *et al.*, 2023).

From a medicinal chemistry perspective, the 1,2,3-triazole ring is regarded as a privileged pharmacophore because of its remarkable metabolic stability, resistance to hydrolytic and oxidative degradation, and ability to participate in hydrogen bonding, dipole–dipole interactions, and π–π stacking with biological macromolecules (Lengerli *et al.*, 2022; Martis *et al.*, 2025; Sharma *et al.*, 2023). Moreover, the triazole nucleus frequently serves as a bioisostere of amide and ester functionalities, thereby enhancing receptor binding while improving pharmacokinetic properties. These characteristics have contributed significantly to the widespread application

of 1,2,3-triazoles in the rational design of antimicrobial and other therapeutic agents (Kukov *et al.*, 2025).

Recent studies have demonstrated that the incorporation of pharmacologically relevant substituents, such as nitroaromatic groups, ether linkages, and hydrophobic aromatic fragments, can substantially influence antimicrobial activity by modulating lipophilicity, electronic distribution, molecular polarity, and membrane permeability (Akinwumi & Ambali, 2026; Majumder & Panigrahi, 2025). In particular, the *p*-nitrophenoxy moiety represents an attractive pharmacophoric fragment because its strongly electron-withdrawing nitro group can influence molecular polarization and facilitate interactions with biological targets through electronic and redox-related effects (Abreu *et al.,* 2024). Likewise, incorporation of a benzyl substituent on the triazole nitrogen can enhance hydrophobic interactions with microbial membranes and enzyme binding pockets, potentially influencing cellular uptake and biological efficacy. Collectively, the combination of a benzyl substituent and an electron-deficient nitrophenoxy group linked through a rigid triazole core generates a donor–acceptor molecular architecture with potentially favourable electronic and intermolecular interaction characteristics (Agarwal *et al.,* 2025).

Although relatively few clinically approved antimicrobial agents contain a true 1,2,3-triazole nucleus, in contrast to the widely prescribed 1,2,4-triazole antifungal drugs such as fluconazole, voriconazole, and posaconazole, the 1,2,3-triazole scaffold has nevertheless emerged as a highly valuable structural motif in antimicrobial drug discovery (Lu *et al.,* 2025; Teixeira *et al.,* 2022). Numerous experimental studies have demonstrated that appropriately substituted 1,2,3-triazole derivatives exhibit potent antibacterial and antifungal activities against both Gram-positive and Gram-negative pathogens, highlighting the importance of strategic structural modification in optimizing biological performance (Vaishnani *et al.,* 2024).

Despite these promising advances, systematic investigations of benzyl-substituted 1,2,3-triazoles incorporating nitrophenoxy functionalities through an ether-methylene spacer remain scarce. Furthermore, most reported triazole-based antimicrobial agents either focus on relatively simple substitution patterns or do not systematically investigate the synergistic influence of electron-withdrawing aromatic substituents, flexible ether linkages, and hydrophobic benzyl groups within a single molecular framework. Consequently, the relationship between these structural features and antimicrobial activity remains insufficiently understood, limiting the rational design of more potent triazole-based antimicrobial agents.

In the present study, we report the design and synthesis of the novel 1,2,3-triazole derivative 1-benzyl-4-((4-nitrophenoxy)methyl)-1H-1,2,3-triazole, prepared through a modular CuAAC click chemistry strategy involving benzyl azide and 1-nitro-4-(prop-2-yn-1-yloxy)benzene as the key building blocks. The molecular design integrates three complementary structural elements: (i) a chemically robust 1,2,3-triazole nucleus serving as the central pharmacophore, (ii) a benzyl substituent intended to influence lipophilicity and hydrophobic interactions, and (iii) a *p*-nitrophenoxy fragment introduced to modulate the electronic characteristics of the molecule and potentially influence biological activity. The synthesized compound was comprehensively characterized using FTIR, UV–Visible spectroscopy, ^{1}H and ^{13}C NMR spectroscopy, and high-resolution mass spectrometry (HRMS), followed by evaluation of its antibacterial and antifungal activities against selected Gram-positive, Gram-negative, and fungal microorganisms.

MATERIALS AND METHODS

Chemicals and Reagents

All chemicals used in this study were of analytical grade and included benzyl chloride, sodium azide, acetone, propargyl bromide, potassium carbonate, 4-nitrophenol, copper(II) sulphate pentahydrate, sodium ascorbate, and dimethylformamide (DMF). All reagents were used as received without further purification unless otherwise stated.

Physicochemical and analytical characterization of the synthesized compound was carried out using standard techniques. Nuclear magnetic resonance (NMR) spectra were recorded on a Bruker 500 MHz spectrometer, operating at 500 MHz for ^{1}H and 125 MHz for ^{13}C NMR. DMSO-d_6 was used as the solvent for all measurements, and proton decoupling was applied during ^{13}C NMR analysis. Chemical shifts (δ) are reported in parts per million (ppm) relative to DMSO-d_6, with reference values of $\delta_H = 2.50$ppm and $\delta_C = 39.50$ppm. All NMR measurements were performed at room temperature. Infrared (IR) spectra were recorded using either a Bruker Tensor 27 or a PerkinElmer FT-IR spectrometer. Elemental analyses were carried out using a Vario EL III CHN analyzer. High-resolution mass spectra (HRMS) were obtained using a Waters Acquity UPLC Synapt G2 HD mass spectrometer.

Synthesis

The primary objective of this study was to synthesize 1-benzyl-4-((4-nitrophenoxy)methyl)-*1H-1,2,3-triazole* via a click chemistry approach (Oprea & Smith, 2024). The target compound was prepared through a three-step synthetic route, comprising the formation of benzyl azide and a propargylated nitrophenol intermediate from benzyl chloride and 4-nitrophenol precursors, respectively, followed by a copper(I)-catalyzed azide–alkyne cycloaddition (CuAAC) reaction to afford the desired 1,2,3-triazole derivative (Bhatia *et al.,* 2025). The step-by-step synthetic procedures for the preparation of the intermediates and the final compound are outlined below.

Synthesis of (azidomethyl)Benzene

Sodium azide (2.0 g, 30.77 mmol, 1.5 equiv.) and benzyl chloride (2.60 g, 20.51 mmol, 1.0 equiv.) were dissolved in a mixture of acetone and water (100 mL, 2:1 v/v). The reaction mixture was stirred at 65 °C until completion, as monitored by thin-layer chromatography (TLC).

Upon completion, the reaction mixture was filtered and extracted with ethyl acetate (15 mL). The organic phase was washed with deionized water (3 × 10 mL), dried over anhydrous sodium sulphate, filtered, and concentrated under reduced pressure. The resulting product was further dried under vacuum and characterized by ^{1}H and ^{13}C NMR spectroscopy to confirm its structure before use in subsequent reactions. The synthetic route is illustrated in Figure 1.

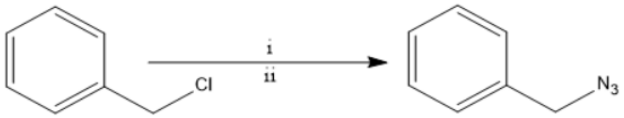

Figure 1: Synthetic Route for the Preparation of (azidomethyl) Benzene, the Azide Partner for the Click Chemistry Reaction. Reagents and Conditions: (i) NaN_3; (ii) Acetone/Water (10:5, v/v), 65 °C, 4 h

Extracted Spectral Data

(Azidomethyl)benzene: Pale yellow oil; yield: 2.51 g (92%). ^{1}H NMR (500 MHz, DMSO-d_6): δ 7.42 (d, J = 7.5 Hz, 1H, Ar-H), 7.39 (d, J = 8.5 Hz, 2H, Ar-H), 7.35 (t, J = 8.5 Hz, 2H, Ar–H), 4.42 (s, 2H, CH_2N_3). ^{13}C NMR (125 MHz, DMSO-d_6): δ 135.49 (Grady et al.), 128.52, 128.22, 127.95 (Ar–CH), 53.69 (CH_2N_3), (Appendix S3-4).

Synthesis of 1-nitro-4-(prop-2-yn-1-yloxy) Benzene

1-Nitro-4-(prop-2-yn-1-yloxy)benzene was synthesized from 4-nitrophenol *via* O-propargylation using a reported literature procedure with slight modification (Kaur *et al.,* 2021). Briefly, 4-nitrophenol (2.50 g, 17.98 mmol, 1 equiv.) was dissolved in 100 mL of acetone, after which potassium carbonate (3.72 g, 26.97 mmol, 1.5 equiv.) was added. The resulting suspension was stirred at 65 °C for 1 h to facilitate deprotonation of the phenolic hydroxyl group. Subsequently, propargyl bromide (3.21 g, 26.97 mmol, 1.5 equiv.) was added dropwise under continuous stirring. After complete addition, the reaction mixture was maintained at 65 °C for an additional 4 h, with the progress of the reaction monitored periodically by thin-layer chromatography (TLC) using a hexane/ethyl acetate (2:8, v/v) solvent system until complete consumption of the starting material.

Upon completion, the reaction mixture was allowed to cool to room temperature, and the solvent was removed under reduced pressure using a rotary evaporator. The resulting crude product was dissolved in 100 mL of ethyl acetate and washed with distilled water (3 × 50 mL) to remove inorganic salts and other water-soluble impurities. The organic layer was dried over anhydrous magnesium sulphate, filtered, and concentrated under reduced pressure to afford the alkylated product as a brown solid. The synthesized compound was subsequently characterized by ^{1}H and ^{13}C NMR spectroscopy to confirm its successful formation. The corresponding spectral data are presented in supplementary information, while the synthetic route is illustrated in Figure 2.

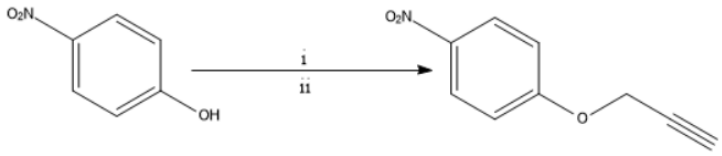

Figure 2: Synthetic route for the preparation of 1-nitro-4-(prop-2-yn-1-yloxy) benzene, the alkyne partner for the click chemistry reaction. Reagents and conditions: (i) K_2CO_3, propargyl bromide; (ii) acetone, 65 °C, 5 h.

Extracted Spectral Data

1-Nitro-4-(prop-2-yn-1-yloxy)benzene: Brown solid; yield: 2.30 g (72.3%); m.p.: 112–114 °C. ^{1}H NMR (500 MHz, DMSO-d_6): δ 8.36 (d, J = 9.0 Hz, 2H, Ar–H), 8.20 (d, J = 9.0 Hz, 2H, Ar–H), 5.02 (s, 2H, OCH_2), 3.66 (s, 1H, C≡CH). ^{13}C NMR (125 MHz, DMSO-d_6): δ 163.52 (Ar–O), 150.38 (Ar–NO_2), 134.31 (2 × Ar–CH), 123.90 (2 × Ar–CH), 78.33 (C≡CH), 53.25 (OCH_2), (Appendix S7-8).

Synthesis of 1-benzyl-4-((4-nitrophenoxy)methyl)-1*H*-1,2,3-triazole

1-Benzyl-4-((4-nitrophenoxy)methyl)-*1H-1,2,3-triazole* was synthesized via a copper(I)-catalyzed azide–alkyne cycloaddition (CuAAC) reaction. Briefly, 1-nitro-4-(prop-2-yn-1-yloxy)benzene (1.72 g, 9.70 mmol, 1 equiv.) was dissolved in a DMF/H_2O mixture (100 mL, 4:1, v/v). To this solution, (azidomethyl)benzene (1.56 g, 11.70 mmol, 1.2 equiv.) was added, followed by an aqueous solution of $CuSO_4 \cdot 5H_2O$ (0.015 g, 0.060 mmol in 1 mL of water) and sodium ascorbate (0.174 g, 0.880 mmol in 2 mL of water). The resulting reaction mixture was stirred at 80 °C for 24 h, with the progress of the reaction monitored by thin-layer chromatography (TLC).

Upon completion, the reaction mixture was poured into an ice-water mixture, resulting in the formation of a precipitate. The solid product was collected by vacuum filtration, washed with ice-cold water (3 × 25 mL), and dried to afford 1-benzyl-4-((4-nitrophenoxy)methyl)-*1H-1,2,3-triazole* as a cream-colored solid.

The synthesized compound was characterized by ^{1}H NMR, ^{13}C NMR, FTIR, UV–Vis, and high-resolution mass spectrometry (HRMS) to confirm its structure. The corresponding spectral data are presented below, while the synthetic route is illustrated in Figure 3.

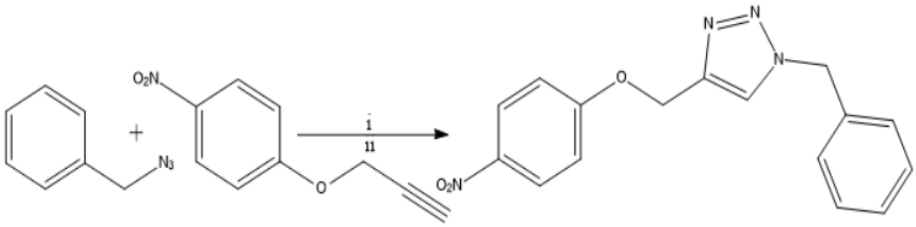

Figure 3: Synthetic Route for the Preparation of 1-benzyl-4-((4-nitrophenoxy)methyl)-1*H*-1,2,3-triazole *via* Cu(I)-catalyzed azide–alkyne Cycloaddition (CuAAC). Reagents and Conditions: (i) $CuSO_4 \cdot 5H_2O$, Sodium Ascorbate; (ii) DMF/H_2O (4:1, v/v), 80 °C, 24 h.

Extracted Spectral Data

1-Benzyl-4-((4-nitrophenoxy)methyl)-1*H*-1,2,3-triazole:
Cream-colored solid; yield: 2.52 g (83.2%); m.p.: 248–252 °C. ^{1}H NMR (500 MHz, DMSO-d_6): δ 8.34 (d, J = 9.0 Hz, 2H, Ar–H), 8.18 (s, 1H, triazole-H), 8.16 (d, J = 9.0 Hz, 2H, Ar–H), 7.40–7.33 (m, 5H, Ar–H), 5.62 (s, 2H, NCH_2Ph), 5.45 (s, 2H, OCH_2). ^{13}C NMR (125 MHz, DMSO-d_6): δ 163.93 (Ar–O), 150.27 (Ar–NO_2), 141.61 (triazole C), 135.95 (ipso-Ar), 130.69, 130.26, 128.10, 127.95, 125.04, 123.83 (Ar–C), 58.62 (OCH_2), 52.08 (NCH_2Ph). FTIR (ATR, ν_max, cm^{-1}): 3125 (Ar/Triazole C–H), 2908 (aliphatic C–H), 1720, 1604 (Ar C=C/C=N), 1520 (ν_as(NO_2)), 1435, 1342 (ν_s(NO_2)), 1265 (Ar–O–CH_2), 1095 (C–O–C), 918, 717 (Ar–H out-of-plane). UV–Vis (DMSO): λ_max (nm) = 257 (n→π*), 322 (n→π*), 411 (n→π*). HRMS (ESI$^+$): *m/z* calculated for $C_{16}H_{15}N_4O_3$ $[M+H]^+$, 311.1140; found, 311.2114. Anal. Calcd. (%) for $C_{16}H_{14}N_4O_3$: C, 61.93; H, 4.55; N, 18.06. Found (%): C, 61.88; H, 4.51; N, 17.98.

Biological Study

Antimicrobial Evaluation

The antimicrobial activity of the synthesized 1-benzyl-4-((4-nitrophenoxy)methyl)-1*H*-1,2,3-triazole was evaluated against selected bacterial and fungal strains. The antibacterial and antifungal activities were initially assessed using the disc diffusion assay, while the minimum inhibitory concentration (MIC) and minimum fungicidal concentration (MFC) were determined using the broth microdilution method according to the Clinical and Laboratory Standards Institute (CLSI) guidelines with slight modifications (Armengol *et al.,* 2021; Urbin *et al.,* 2025).

Antibacterial Evaluation

The *in vitro* antibacterial activity of the test compound was evaluated against three Gram-positive bacterial strains, *Staphylococcus aureus*, *Streptococcus pyogenes*, and *Enterococcus faecalis* (formerly *Streptococcus faecalis*), and three Gram-negative bacterial strains, *Escherichia coli*, *Salmonella typhi*, and *Klebsiella pneumoniae*.

Fresh bacterial cultures were adjusted to the 0.5 McFarland turbidity standard (approximately 1.5 × 10^8 CFU mL^{-1}) and uniformly inoculated onto sterile Mueller–Hinton agar (MHA) plates using sterile cotton swabs. Sterile paper discs (6 mm diameter) were impregnated with 20 µL of the test compound prepared in 1% (v/v) dimethyl sulfoxide (DMSO) at concentrations of 100, 50, 25, and 12.5 µg mL^{-1}. The discs were allowed to dry under aseptic conditions before being placed onto the inoculated agar surface. Amoxicillin (12.5 µg mL^{-1}), applied to the discs at the same volume (20 µL), served as the positive control, while 1% (v/v) DMSO, which exhibited no antibacterial activity, was used as the negative control. The inoculated plates were incubated at 37 °C for 24 h, after which the diameters of the inhibition zones were measured in millimetres (mm). All experiments were performed in triplicate, and the results are expressed as mean ± standard deviation.

Antifungal Evaluation

The *in vitro* antifungal activity of the test compound was evaluated against *Candida albicans*, and *Aspergillus fumigatus* using the disc diffusion method. Fresh fungal suspensions were uniformly inoculated onto sterile Sabouraud Dextrose Agar (SDA) plates. Sterile paper discs (6 mm in diameter) were impregnated with 20 µL of the test compound dissolved in 1% (v/v) dimethyl sulfoxide (DMSO) at concentrations of 100, 50, 25, and 12.5 µg mL^{-1}. The discs were allowed to dry under aseptic conditions before being placed on the inoculated agar surface.

Ketoconazole (12.5 µg mL^{-1}), applied to the discs in the same volume (20 µL), served as the positive control, while 1% (v/v) DMSO, which exhibited no antifungal activity, was used as the negative control. The inoculated plates were incubated at 37 °C for 72 h, after which the diameters of the inhibition zones were measured in millimetres (mm). All experiments were performed in triplicate, and the results are expressed as mean ± standard deviation.

Determination of Minimum Inhibitory Concentration (MIC)

The minimum inhibitory concentrations (MICs) of the test compound against the bacterial isolates were determined using the broth microdilution method according to the Clinical and Laboratory Standards Institute (CLSI) M07 guidelines, with slight modifications (Wiegand *et al.,* 2008).

Fresh overnight bacterial cultures were suspended in sterile nutrient broth and adjusted to the 0.5 McFarland turbidity standard, corresponding to approximately 1.5 × 10^8 CFU mL^{-1}. The standardized suspension was subsequently diluted to obtain a final working inoculum of approximately 5 × 10^5 CFU mL^{-1} for the susceptibility assay.

Under aseptic conditions, 100 µL of the standardized bacterial inoculum was dispensed into each well of a sterile 96-well microplate containing 100 µL of serially diluted test compound prepared in nutrient broth to obtain final concentrations of 25, 12.5, 6.25, 3.125, 1.56, 0.78, and 0.39 µg mL^{-1}. The microplates were incubated at 37 °C for 24 h.

Following incubation, 10 µL of 0.02% (w/v) resazurin solution was added to each well, and the plates were incubated for a further 1–2 h to allow colour development. Wells that remained blue indicated complete inhibition of bacterial growth, whereas wells that changed from blue to pink indicated viable bacterial cells due to the reduction of resazurin to resorufin. The MIC was recorded as the lowest concentration of the compound that completely inhibited visible bacterial growth. All determinations were performed in triplicate, and the results are expressed as mean ± standard deviation.

Determination of Minimum Fungicidal Concentration (MFC)

The minimum fungicidal concentration (MFC) of the test compound was determined using the broth microdilution method according to the Clinical and Laboratory Standards Institute (CLSI) M38-A2 guideline for filamentous fungi, with slight modifications (Wiegand *et al.,* 2008). Ketoconazole served as the positive control.

Fresh fungal spore suspensions were prepared and adjusted to approximately 1×10^5 spores mL^{-1}. Aliquots (100 µL) of the fungal suspension were added to 100 µL of serially diluted test compound prepared in Sabouraud Dextrose Broth (SDB) to obtain final concentrations of 25, 12.5, 6.25, 3.125, 1.56, 0.78, and 0.39 µg mL^{-1}. The microplates were incubated at 30 °C for 72 h.

Following incubation, 10 µL of 0.02% (w/v) resazurin solution was added to each well to assess fungal metabolic activity. Wells that remained blue indicated complete inhibition of fungal growth, whereas wells that turned pink indicated metabolically active fungal cells. The MIC was recorded as the lowest concentration of the compound that completely inhibited visible fungal growth.

To determine the MFC, aliquots from all wells showing no visible growth (blue wells) were aseptically subculture onto fresh, drug-free Sabouraud Dextrose Agar (SDA) plates and incubated at 30 °C for a further 72 h. The MFC was defined as the lowest concentration of the compound that produced no visible fungal growth on the drug-free medium, thereby confirming complete fungicidal activity. All experiments were performed in triplicate, and the results are expressed as mean ± standard deviation.

RESULTS AND DISCUSSION

Chemistry

1-Benzyl-4-((4-nitrophenoxy)methyl)-*1H-1,2,3-triazole* (PNT) was synthesized through a three-step synthetic route, as illustrated in figure 4. In the first step, benzyl chloride underwent nucleophilic substitution with sodium azide in acetone to afford benzyl azide as a pale-yellow oil. The reaction proceeded efficiently through displacement of the chloride ion by the azide nucleophile, generating the organic azide required for the subsequent cycloaddition reaction.

In the second step, 4-nitrophenol was subjected to O-propargylation using propargyl bromide in the presence of excess potassium carbonate as the base. Potassium carbonate facilitated deprotonation of the phenolic hydroxyl group, generating the corresponding phenoxide ion, which subsequently underwent nucleophilic substitution with propargyl bromide to yield 1-nitro-4-(prop-2-yn-1-yloxy)benzene, the terminal alkyne precursor, as a brown solid.

The final step involved a copper(I)-catalyzed azide–alkyne cycloaddition (CuAAC), commonly referred to as the *click reaction*, between benzyl azide and the propargylated nitrophenyl ether. The reaction afforded the desired 1,4-disubstituted 1,2,3-triazole, 1-benzyl-4-((4-nitrophenoxy)methyl)-*1H-1,2,3-triazole* (PNT), in an excellent isolated yield of 83.2%. The high yield and clean conversion demonstrate the efficiency and regioselectivity of the CuAAC methodology, which is well known for its mild reaction conditions, broad functional-group tolerance, and reliable formation of 1,4-disubstituted triazoles (Tiwari *et al.,* 2024). The synthesized compound was isolated as a cream-coloured solid and was found to be stable under ambient laboratory conditions. It exhibited good solubility in methanol, ethanol, chloroform, dichloromethane, and acetone, whereas it was insoluble in toluene, hexane, diethyl ether, and ethyl acetate. The observed solubility profile reflects the relatively polar nature of the molecule, which arises from the presence of the 1,2,3-triazole ring, the nitro substituent, and the ether linkage, all of which contribute to increased molecular polarity while maintaining compatibility with moderately polar organic solvents.

The molecular structure of PNT was confirmed using a combination of spectroscopic and analytical techniques, including FTIR, UV–Visible spectroscopy, high-resolution mass spectrometry (HRMS), and NMR spectroscopy. The structural assignments and detailed interpretation of the characterization data are presented and discussed in the spectroscopic characterization sections.

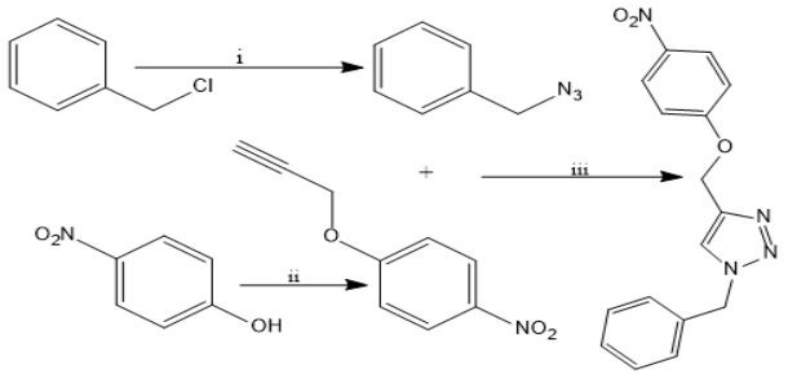

Figure 4: General Route for the Synthesis of 1-benzyl-4-((4-nitrophenoxy)methyl)-*1H-1,2,3-triazole* (PNT). Step (i): Nucleophilic Substitution of Benzyl Chloride with Sodium Azide in Acetone to afford Benzyl Azide. Step (ii): O-propargylation of 4-nitrophenol with Propargyl Bromide in the Presence of Potassium Carbonate to Produce 1-nitro-4-(prop-2-yn-1-yloxy)benzene, the Terminal Alkyne Precursor. Step: copper(I)-catalyzed azide–alkyne Cycloaddition (CuAAC) Between Benzyl Azide and the Terminal Alkyne to Furnish the Target 1,4-disubstituted 1,2,3-triazole (PNT)

Spectroscopic Characterization

Nuclear Magnetic Resonance

The molecular structure of 1-benzyl-4-((4-nitrophenoxy)methyl)-1*H*-1,2,3-triazole (PNT) was confirmed by ^{1}H and ^{13}C NMR spectroscopy recorded in DMSO-*d*6 at 500 MHz and 125 MHz, respectively (Figures 1a and b).

The ^{1}H NMR spectrum exhibited a characteristic singlet at δ 8.34 ppm (1H, s), which was assigned to the proton located at the C5 position of the 1,4-disubstituted 1,2,3-triazole ring. The presence of a single triazole proton is diagnostic of the successful copper(I)-catalyzed azide-alkyne cycloaddition (CuAAC), since formation of the 1,4-disubstituted triazole leaves only one proton on the heterocyclic ring (George *et al.,* 2023b).

The aromatic protons of the 4-nitrophenoxy moiety appeared as two well-resolved doublets centred at approximately δ 8.32 and 8.18 ppm, each integrating for two protons with an ortho coupling constant of approximately J ≈ 9.0 Hz. This AA′BB′ spin system is characteristic of a para-disubstituted benzene ring, confirming the integrity of the *p*-nitrophenoxy fragment after O-propargylation and subsequent cycloaddition.

The benzyl phenyl ring resonated as a triplet between δ 7.39–7.36 ppm, and doublet at 7.34 ppm, integrating for two and three aromatic protons, consistent with a monosubstituted phenyl group attached to the triazole nitrogen.

Two distinct methylene singlets were observed at δ 5.62 and 5.45 ppm, each integrating for two protons. The resonance at δ 5.62 ppm was assigned to the N–CH_2–Ph group attached directly to the triazole nitrogen, while the signal at δ 5.45 ppm corresponded to the O–CH_2–triazole bridge connecting the triazole ring to the nitrophenoxy unit. The appearance of both methylene groups as singlets indicates the absence of vicinal protons available for spin–spin coupling, which is consistent with the proposed molecular structure.

Importantly, the spectrum showed the complete disappearance of the characteristic terminal alkyne proton expected near δ 3.66 ppm for the propargyl precursor, as well as the absence of signals attributable to benzyl azide. These observations provide strong evidence that the cycloaddition reaction proceeded to completion, resulting in formation of the triazole ring.

The ^{13}C NMR spectrum (Figure 5b) further corroborated the proposed structure. The resonance at δ 163.93 ppm was assigned to the aryl C–O carbon bonded to the ether oxygen, while the signal at δ 150.27 ppm corresponded to the quaternary aromatic carbon bearing the nitro substituent. The remaining aromatic carbons appeared within the expected range of δ 123.83–141.61 ppm, consistent with the substituted nitrophenoxy and benzyl phenyl rings.

Signals attributable to the triazole carbons were observed within the aromatic heterocyclic region, with the quaternary triazole carbon appearing around δ 138.66 ppm, in agreement with literature values reported for 1,4-disubstituted 1,2,3-triazoles (Şahin, 2022). The methylene carbons resonated at δ 58.62 ppm (N–CH_2–Ph) and 52.80 ppm (O–CH_2–triazole), confirming the presence of two chemically distinct methylene bridges linking the triazole ring to the benzyl and nitrophenoxy substituents (Singh *et al.,* 2021).

The combined ^{1}H and ^{13}C NMR data provide evidence for the successful synthesis of 1-benzyl-4-((4-nitrophenoxy)methyl)-1*H*-1,2,3-triazole (PNT). The appearance of the diagnostic triazole proton, the characteristic AA′BB′ aromatic pattern of the *p*-nitrophenoxy group, the two distinct methylene singlets linking the triazole to the benzyl and aryloxy fragments, together with the disappearance of the terminal alkyne proton and the expected carbon resonances in the ^{13}C NMR spectrum, confirm the successful formation of the desired 1,4-disubstituted 1,2,3-triazole.

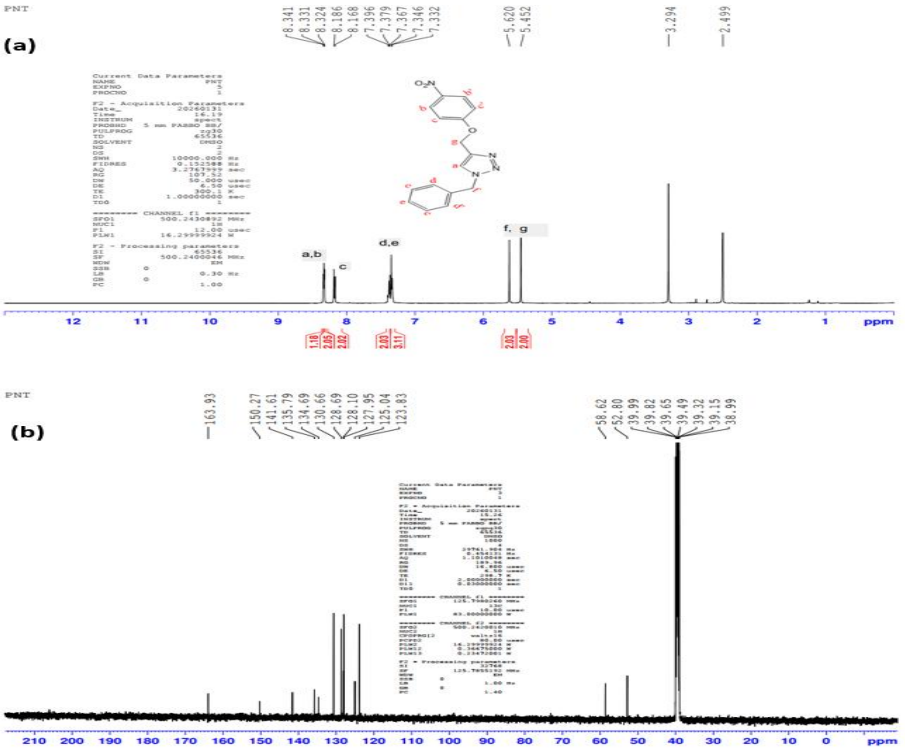

Figure 5: NMR Characterization of 1-benzyl-4-((4-nitrophenoxy)methyl)-1*H*-1,2,3-Triazole (PNT) Recorded in DMSO-*d*6: (a) ^{1}H NMR Spectrum (500 MHz) with Assigned Proton Resonances; (b) ^{13}C NMR Spectrum (125 MHz) Showing the Corresponding Carbon Resonances that Verify the Molecular Structure of the Synthesized Triazole Derivative

Fourier Transform Infrared (FTIR) Spectroscopy

The FTIR spectrum of 1-benzyl-4-((4-nitrophenoxy)methyl)-1*H*-1,2,3-triazole (PNT) is presented in Figure 6, and the principal absorption bands are consistent with the proposed molecular structure. A weak absorption observed at 3125 cm^{-1} is assigned to the aromatic and heteroaromatic C–H stretching vibrations associated with the phenyl and triazole rings. The band at 2908 cm^{-1} corresponds to the aliphatic C–H stretching vibrations of the methylene (–CH_2–) groups linking the triazole ring to the benzyl and nitrophenoxy substituents.

A prominent absorption band at 1604 cm^{-1} is attributed to the C=N stretching vibration of the 1,2,3-triazole ring together with contributions from aromatic C=C stretching vibrations. The strong absorptions observed at 1520 cm^{-1} and 1342 cm^{-1} are characteristic of the asymmetric and symmetric stretching vibrations of the nitro (–NO_2) group, respectively, confirming the retention of the para-nitrophenyl moiety following the cycloaddition reaction. The additional band at 1435 cm^{-1} is assigned to aromatic ring skeletal vibrations and methylene bending modes.

The intense absorption at 1265 cm^{-1} is assigned to the aryl–O–CH_2 ether (C–O–C) stretching vibration, confirming the presence of the ether linkage connecting the nitrophenyl ring to the methylene bridge. A second strong band at 1095 cm^{-1} is attributed to C–O stretching together with contributions from C–N stretching within the triazole framework. The absorption at 918 cm^{-1} is associated with out-of-plane bending vibrations of aromatic C–H bonds and vibrations of the substituted triazole ring, while the band at 717 cm^{-1} corresponds to the out-of-plane bending vibration of the monosubstituted benzyl phenyl ring. The absorption observed at 493 cm^{-1} is assigned to skeletal deformation vibrations involving the aromatic and heterocyclic framework (Salma *et al.*, 2025).

More importantly, the FTIR spectrum provides evidence for the successful copper(I)-catalyzed azide–alkyne cycloaddition (CuAAC). The characteristic azide stretching vibration expected near 2100–2150 cm^{-1} for the benzyl azide precursor is absent in the final product. Likewise, the terminal alkyne ≡C–H stretching band typically observed around 3250–3300 cm^{-1} and the C≡C stretching vibration expected within 2100–2140 cm^{-1} are no longer present. The disappearance of these diagnostic bands, together with the appearance of the characteristic triazole-associated absorption at 1604 cm^{-1}, confirms complete consumption of both click reaction precursors and successful formation of the desired 1,4-disubstituted 1,2,3-triazole.

The FTIR data agree with the proposed structure of PNT and complement the NMR and HRMS analyses in confirming the successful synthesis of the target triazole derivative.

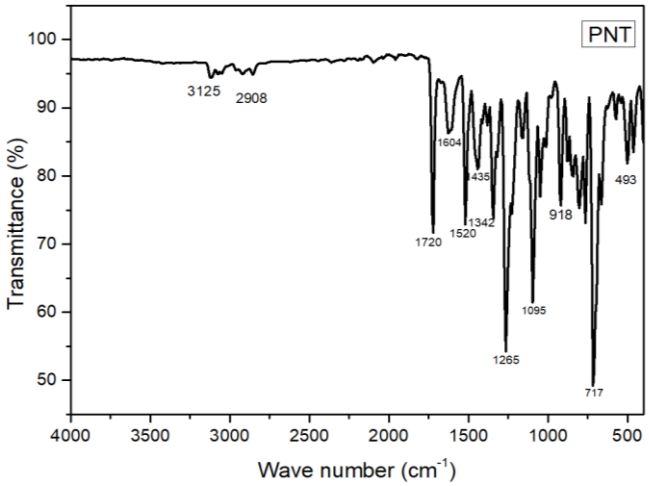

Figure 6: FTIR Spectrum of 1-benzyl-4-((4-nitrophenoxy)methyl)-*1H-1,2,3-triazole* (PNT) Recorded over the Spectral Range of 4000–400 cm^{-1}, Showing the Characteristic Absorption Bands Corresponding to the Triazole, Nitro, Aromatic, Ether, and Methylene Functional Groups

UV–Visible Spectroscopy

The electronic absorption spectrum of 1-benzyl-4-((4-nitrophenoxy)methyl)-1*H*-1,2,3-triazole (PNT), recorded in DMSO, is presented in Figure 7. The spectrum exhibits three well-defined absorption bands centred at 257, 322, and 411 nm, corresponding to the characteristic electronic transitions associated with the conjugated aromatic and heterocyclic framework of the molecule.

The intense absorption band at 257 nm is assigned to the π→π* electronic transition of the aromatic phenyl rings and the conjugated 1,2,3-triazole system. Such high-energy transitions are typical of aromatic compounds containing extended π-electron systems and indicate efficient delocalization of π-electrons throughout the molecular framework.

A second absorption band at 322 nm is attributed primarily to π→π* transitions involving the conjugated 4-nitrophenoxy moiety. The presence of the strongly electron-withdrawing nitro group, together with the electron-donating ether oxygen, enhances conjugation across the aromatic ring, resulting in a bathochromic shift relative to unsubstituted aromatic systems. In addition, conjugation between the triazole ring and the aryloxy substituent contributes to the observed absorption in this region (George *et al.*, 2023a).

The lower-energy absorption observed at 411 nm is assigned to an intramolecular charge-transfer transition with contributions from n→π* excitation associated with the nitro group. This transition arises from electron donation by the electron-rich aryloxy oxygen and triazole ring toward the electron-deficient nitro-substituted aromatic ring, producing a donor–π–acceptor (D–π–A) electronic system. The appearance of this visible-region absorption is indicative of efficient electronic communication across the molecule and

confirms the establishment of an extended conjugated framework following formation of the triazole ring.

Compared with the individual synthetic precursors, the emergence of the absorption band at 411 nm and the enhanced absorption at 322 nm indicate increased molecular conjugation resulting from the CuAAC reaction. Formation of the 1,2,3-triazole bridge extends the π-electron delocalization between the benzyl and nitrophenoxy fragments, thereby lowering the energy required for electronic excitation and producing the observed bathochromic effect.

Overall, the UV–Visible spectrum is consistent with the proposed molecular structure of PNT and supports the successful formation of the 1,4-disubstituted 1,2,3-triazole. The observed electronic transitions reflect the combined influence of the aromatic rings, triazole heterocycle, ether linkage, and nitro substituent on the electronic properties of the molecule.

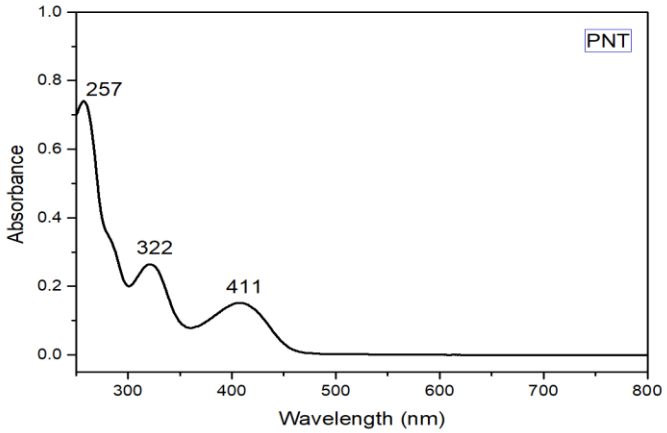

Figure 7: UV–Visible Absorption Spectrum of 1-benzyl-4-((4-nitrophenoxy)methyl)-*1H-1,2,3-triazole* (PNT) Recorded in DMSO, Showing the Characteristic Absorption Maxima at 257, 322, and 411 nm, Assigned to the π→π* Transitions of the Aromatic/Triazole Chromophores and the Intramolecular Charge-Transfer (Lionetti et al.)/n→π* Transition Associated with the Conjugated Nitrophenoxy–Triazole Framework

High-Resolution Mass Spectrometry (HRMS)

The molecular composition of 1-benzyl-4-((4-nitrophenoxy)methyl)-1*H*-1,2,3-triazole (PNT) was further confirmed by high-resolution electrospray ionization time-of-flight mass spectrometry (HR-ESI-TOF-MS), and the spectrum is presented in Figure 8. The spectrum exhibits a prominent molecular ion peak at m/z 311.2114, corresponding to the protonated molecular ion $[M+H]^+$. This value closely agrees with the calculated exact mass of m/z 311.1144 for the proposed molecular formula.

The close agreement between the calculated and experimental masses confirms the molecular weight and elemental composition of the synthesized triazole derivative. Moreover, the absence of significant competing molecular ion peaks attributable to the benzyl azide, or propargylated precursor indicates that the CuAAC reaction proceeded efficiently to completion, yielding the desired product with high purity.

The observed protonated molecular ion is consistent with the expected ionization behaviour of nitrogen-containing heterocyclic compounds under positive electrospray ionization (ESI^+), where protonation preferentially occurs at the electron-rich nitrogen atoms of the 1,2,3-triazole ring. The high mass accuracy obtained from the TOF analyzer therefore provides strong analytical evidence for the successful formation of 1-benzyl-4-((4-nitrophenoxy)methyl)-1*H*-1,2,3-triazole, complementing the structural information obtained from FTIR, UV–Visible, and NMR spectroscopic analyses.

Collectively, the HRMS data confirm that the isolated product possesses the expected molecular composition and further validate the successful synthesis of the target 1,4-disubstituted 1,2,3-triazole.

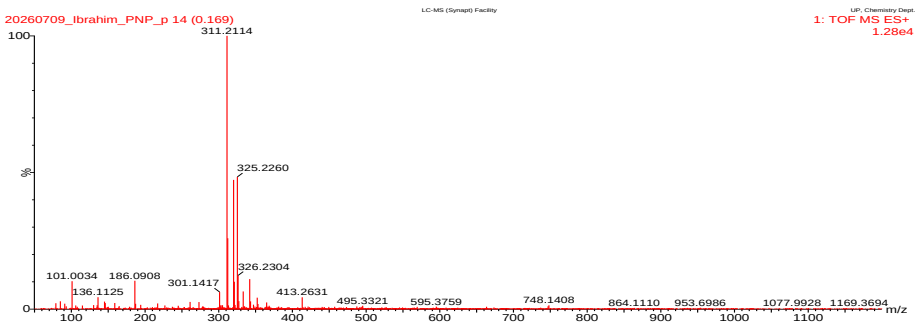

Figure 8: Positive-ion HR-ESI-TOF Mass Spectrum of 1-benzyl-4-((4-nitrophenoxy)methyl)-1*H*-1,2,3-triazole (PNT) Showing the Protonated Molecular ion $[M+H]^+$ at m/z 311.1114, in a Close Agreement with the Calculated Exact Mass (m/z 311.2114), Confirming the Molecular Composition of the Synthesized Triazole Derivative

Biological Evaluation

Antimicrobial Study

Following the successful synthesis of 1-benzyl-4-((4-nitrophenoxy)methyl)-*1H-1,2,3-triazole* (PNT), as confirmed by the spectroscopic characterization, its antimicrobial activity was evaluated using the agar well diffusion method. The compound was screened against six clinically relevant bacterial strains, comprising three Gram-positive bacteria (*Staphylococcus aureus*, *Streptococcus pyogenes*, and *Streptococcus faecalis*) and three Gram-negative bacteria (*Escherichia coli*, *Salmonella typhi*, and *Klebsiella pneumoniae*), together with two fungal strains (*Candida albicans* and *Aspergillus fumigatus*). These microorganisms were selected to provide a preliminary assessment of the broad-spectrum antimicrobial potential of PNT against pathogens that differ in cell wall architecture and are commonly associated with human infections. The inhibition zone diameters obtained at four concentrations (100, 50, 25, and 12.5 µg/mL) are presented in Table 1, while the corresponding activity indices relative to the standard antimicrobial drugs at 12.5 µg/mL are shown in Figure 9. For comparison, the reference drugs (amoxicillin for bacteria and ketoconazole for fungi), which are clinically approved antimicrobial agents, were evaluated only at 12.5 µg/mL, enabling the relative antimicrobial efficacy of PNT to be assessed under identical experimental conditions.

As shown in Table 1, PNT exhibited measurable antimicrobial activity against all tested bacterial strains at concentrations ranging from 25 to 100 µg/mL, with inhibition zones generally increasing as the concentration increased. This concentration-dependent response indicates that antimicrobial efficacy is directly related to the amount of compound available to diffuse through the agar medium and interact with microbial cells. Such behaviour is characteristic of diffusion-based antimicrobial assays and suggests that PNT possesses intrinsic antimicrobial properties rather than producing random inhibitory effects.

Among the bacterial isolates, *Klebsiella pneumoniae* demonstrated the highest susceptibility toward PNT, with inhibition zones of 18.00 ± 0.26 mm at 100 µg/mL and 12.00 ± 0.26 mm at 12.5 µg/mL. *Staphylococcus aureus* also exhibited appreciable susceptibility, producing inhibition zones ranging from 16.50 ± 0.50 mm at the highest concentration to 10.00 ± 0.62 mm at the lowest concentration. Moderate activity was observed against *Streptococcus pyogenes*, *Salmonella typhi*, and *Escherichia coli*, whereas *Streptococcus faecalis* was the least susceptible bacterium, with complete loss of activity at 12.5 µg/mL. These observations suggest that differences in bacterial cell envelope composition, membrane permeability, and intrinsic resistance mechanisms may influence the susceptibility of individual microorganisms toward the synthesized triazole derivative.

The compound also demonstrated antifungal activity, although the response differed between the two fungal species investigated. *Aspergillus fumigatus* remained susceptible across all tested concentrations, displaying inhibition zones between 17.00 ± 0.56 mm and 11.00 ± 0.26 mm, whereas *Candida albicans* exhibited only moderate inhibition at higher concentrations and no detectable inhibition at 12.5 µg/mL. This difference may reflect variations in fungal cell wall architecture, membrane composition, or cellular uptake of the compound, which collectively influence susceptibility (Gow, 2025).

The observed inhibition zones were expectedly lower than those of the clinically established reference drugs, since amoxicillin and ketoconazole are optimized antimicrobial agents with well-defined molecular targets, whereas PNT represents a newly synthesized triazole derivative undergoing preliminary biological evaluation. Nevertheless, the measurable inhibitory activity observed against both bacterial and fungal pathogens demonstrate that the triazole scaffold possesses promising intrinsic antimicrobial properties and may serve as a valuable lead structure for further structural optimization

To facilitate direct comparison of the antimicrobial efficacy of PNT with the corresponding standard drugs, the Activity Index (AI) was calculated using the equation:

$$\text{Activity Index (\%)} = \frac{\text{Mean inhibition zone of PNT}}{\text{Mean inhibition zone of the reference drug}} \times 100$$

where amoxicillin served as the reference antibacterial agent and ketoconazole as the reference antifungal agent.

The calculated activity indices are summarized in Figure 9. The highest activity indices were observed against *Aspergillus fumigatus* (44.0%) and *Staphylococcus aureus* (43.5%), indicating that PNT retained approximately 44% of the activity of the corresponding standard drugs at the same concentration. Relatively high activity was also observed against *Klebsiella pneumoniae* (37.5%), while moderate activity was recorded against *Streptococcus pyogenes* (29.6%), *Salmonella typhi* (28.6%), and *Escherichia coli* (22.6%). No activity was detected against *Streptococcus faecalis* and *Candida albicans* at 12.5 µg/mL, resulting in activity indices of zero. The activity index analysis provides a normalized assessment of antimicrobial performance and clearly demonstrates that PNT exhibits greater relative efficacy against certain Gram-positive bacteria, *Klebsiella pneumoniae*, and *Aspergillus fumigatus* than against the remaining test organisms.

These results demonstrate that the newly synthesized triazole derivative possesses broad-spectrum antimicrobial activity with concentration-dependent inhibition against both bacterial and fungal pathogens. Although its potency remains lower than that of the established antimicrobial drugs used as positive controls, the compound exhibits promising intrinsic biological activity that could be further enhanced through structural optimization. The present results therefore identify PNT as a useful lead scaffold for the development of new triazole-based antimicrobial agents.

Table 1: Antimicrobial Activity of 1-benzyl-4-((4-nitrophenoxy)methyl)-1*H*-1,2,3-triazole (PNT) Comparative to Control (Amoxicillin and Ketoconazole) Expressed as Inhibition Zone Diameter (mm, mean ± SD, n = 3)

Compounds	**PNT**				**Amoxicillin**	**Ketoconazole**
Microorganism/Conc. (µg/mL)	**100**	**50**	**25**	**12.5**	**12.5**	**12.5**
Staphylococcus aureus	16.50 ± 0.50	13.17 ± 0.76	11.67 ± 0.76	10.00 ± 0.62	23.00 ± 0.26	NA
Streptococcus pyogenes	14.00 ± 0.50	12.00 ± 1.32	10.00 ± 0.26	8.00 ± 0.26	27.00 ± 0.26	NA
Streptococcus faecalis	12.00 ± 0.44	10.00 ± 0.10	7.00 ± 0.50	0.00 ± 0.00	21.67 ± 0.15	NA
Escherichia coli	13.00 ± 0.10	11.33 ± 1.19	9.00 ± 0.10	7.00 ± 0.26	31.00 ± 0.50	NA

Compounds	**PNT**				**Amoxicillin**	**Ketoconazole**
Microorganism/Conc. (µg/mL)	**100**	**50**	**25**	**12.5**	**12.5**	**12.5**
Salmonella typhi	14.00 ± 0.50	12.00 ± 0.26	10.00 ± 0.26	8.00 ± 0.26	28.00 ± 0.26	NA
Klebsiella pneumoniae	18.00 ± 0.26	16.00 ± 0.26	14.00 ± 0.61	12.00 ± 0.26	32.00 ± 0.26	NA
Candida albicans	12.00 ± 0.26	11.00 ± 0.26	7.00 ± 0.26	0.00 ± 0.00	NA	30.00 ± 0.50
Aspergillus fumigatus	17.00 ± 0.56	15.00 ± 0.26	13.00 ± 0.44	11.00 ± 0.26	NA	25.00 ± 0.62

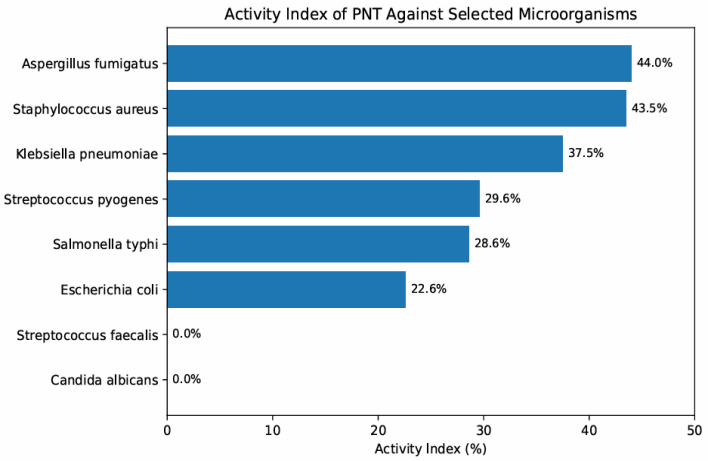

Figure 9: Activity index (%) of 1-benzyl-4-((4-nitrophenoxy)methyl)-1*H*-1,2,3-triazole (PNT) Against Selected Bacterial and Fungal Strains at 12.5 µg/mL, Expressed Relative to the Corresponding Reference Antimicrobial Drug

Minimum Inhibitory Concentration

To further evaluate the antimicrobial potency of PNT, the minimum inhibitory concentration (MIC), minimum bactericidal concentration (MBC), and minimum fungicidal concentration (MFC) were determined against susceptible microorganisms, and the results are summarized in Table 2. The MIC assay provides a quantitative measure of the lowest concentration required to inhibit visible microbial growth, whereas the MBC and MFC values indicate the minimum concentrations required to achieve bactericidal and fungicidal effects, respectively.

As presented in Table 2, PNT exhibited the greatest antibacterial potency against *Staphylococcus aureus*, with both the MIC and MBC recorded at 1.56 µg/mL. The identical MIC and MBC values indicate that the inhibitory concentration was also sufficient to produce a bactericidal effect, suggesting that PNT acts as a bactericidal rather than merely bacteriostatic agent against this organism. A similar relationship between MIC and MBC was observed for *Klebsiella pneumoniae* (3.13 µg/mL) and for *Streptococcus pyogenes*, *Escherichia coli*, and *Salmonella typhi* (6.25 µg/mL), indicating effective killing of these organisms at their respective inhibitory concentrations.

Among the bacterial isolates, *Staphylococcus aureus* was the most susceptible microorganism, followed by *Klebsiella pneumoniae*, whereas *Streptococcus pyogenes*, *Escherichia coli*, and *Salmonella typhi* exhibited moderate susceptibility. In contrast, *Streptococcus faecalis* showed no detectable inhibitory or bactericidal response within the concentration range investigated, corroborating the agar diffusion results (Table 1), where no inhibition zone was observed at the lowest concentration. This consistency between the diffusion and dilution assays strengthens the reliability of the antimicrobial findings.

The antifungal evaluation revealed contrasting responses between the two fungal species. *Aspergillus fumigatus* demonstrated appreciable susceptibility, with both the MIC and MFC determined as 1.56 µg/mL, indicating that PNT exerted fungicidal activity at its minimum inhibitory concentration. Conversely, *Candida albicans* showed no measurable inhibition under the experimental conditions, suggesting intrinsic tolerance or reduced susceptibility to the compound. The observed difference between the two fungal species may be attributed to variations in cell wall composition, membrane sterol content, permeability, and other physiological characteristics that influence the uptake and intracellular activity of antimicrobial agents (Gow, 2025). The MIC, MBC, and MFC data complement the agar diffusion results by providing quantitative evidence of the antimicrobial potency of PNT. The low MIC and MBC values obtained against *Staphylococcus aureus* and *Klebsiella pneumoniae*, together with the fungicidal activity observed against *Aspergillus fumigatus*, demonstrate that the synthesized triazole derivative possesses promising antimicrobial efficacy. Furthermore, the equality of the MIC and MBC/MFC values for susceptible microorganisms suggests that PNT exerts a microbicidal effect at its minimum inhibitory concentration, an attribute that is particularly desirable in the development of new antimicrobial agents. Although inactive against *Streptococcus faecalis* and *Candida albicans*, the compound displayed activity against both Gram-positive and Gram-negative bacteria as well as a filamentous fungus, highlighting its potential as a broad-spectrum antimicrobial scaffold for further structural optimization and mechanistic investigation.

Table 2: Minimum Inhibitory Concentration (MIC), Minimum Bactericidal Concentration (MBC), and Minimum Fungicidal Concentration (MFC) of PNT Against the Test Microorganisms

Microorganism	MIC	MBC	MFC
Staphylococcus aureus	1.56	1.56	–
Streptococcus pyogenes	6.25	6.25	–
Streptococcus faecalis	–	–	–
Escherichia coli	6.25	6.25	–
Salmonella typhi	6.25	6.25	–
Klebsiella pneumoniae	3.13	3.13	–
Candida albicans	–	–	–
Aspergillus fumigatus	1.56	–	1.56

Note: Values are Expressed in µg/mL. "–" Indicates that No Inhibitory, Bactericidal, or Fungicidal Activity was Observed at the Concentrations Investigated

Proposed Structural Rationale for Antimicrobial Activity

Although only a single triazole derivative was evaluated in the present study, several structural features may account for its observed antimicrobial activity. The 1,2,3-triazole ring constitutes a privileged heterocyclic scaffold capable of participating in hydrogen-bonding and dipolar interactions with microbial biomolecular targets while enhancing metabolic stability (Bonandi *et al.,* 2017). The para-nitrophenoxy moiety introduces a strongly electron-withdrawing substituent that modifies the electronic distribution of the aromatic system and may facilitate interactions with microbial enzymes or membrane-associated proteins (Jaber *et al.,* 2025). Furthermore, the benzyl substituent contributes hydrophobic character, potentially promoting membrane permeation and π–π interactions with hydrophobic residues within biological targets (Pal *et al.,* 2022). The combined electronic and hydrophobic effects of these pharmacophoric fragments may account for the broad-spectrum antimicrobial activity observed against both Gram-positive and Gram-negative bacteria as well as *Aspergillus fumigatus*. Nevertheless, because only one compound was investigated, these interpretations should be regarded as a preliminary structure–activity rationale rather than a definitive structure–activity relationship. Future studies involving structurally related analogues, molecular docking, and mechanistic investigations will be required to establish the specific structural determinants governing antimicrobial potency.

CONCLUSION

1,2,3-triazole derivative, 1-benzyl-4-((4-nitrophenoxy)methyl)-1*H*-1,2,3-triazole (PNT), was successfully synthesized through an efficient Cu(I)-catalyzed azide–alkyne cycloaddition reaction and unambiguously characterized by FTIR, UV–Vis, NMR, and HRMS analyses. The spectroscopic data confirmed the successful formation of the target molecule and its proposed molecular structure.

Biological evaluation demonstrated that PNT possesses broad-spectrum antimicrobial activity against both Gram-positive and Gram-negative bacteria, as well as *Aspergillus fumigatus*, with antimicrobial efficacy increasing in a concentration-dependent manner. Quantitative MIC, MBC, and MFC analyses further established the compound's antimicrobial potency, particularly against *Staphylococcus aureus* and *Aspergillus fumigatus*, where inhibitory and microbicidal concentrations were identical (1.56 µg/mL), indicating bactericidal and fungicidal activity at the minimum inhibitory concentration. Activity index analysis confirmed appreciable relative efficacy compared with the corresponding standard antimicrobial agents, especially against *Aspergillus fumigatus*, *Staphylococcus aureus*, and *Klebsiella pneumoniae*. Although the antimicrobial activity remained lower than that of the clinically established reference drugs, the combined presence of the 1,2,3-triazole ring, benzyl substituent, and electron-withdrawing nitrophenoxy moiety provides a plausible structural basis for the observed biological activity. The results demonstrate that PNT represents a promising triazole-based lead scaffold for antimicrobial drug discovery. Future work should focus on the synthesis of structurally related analogues to establish definitive structure-activity relationships, together with molecular docking, mechanistic investigations, cytotoxicity evaluation, and in vivo studies to further assess its therapeutic potential.

ACKNOWLEDGEMENT

Dr. Ibrahim Waziri gratefully acknowledges the University of Johannesburg, through its University Research Centre, for the provision of a postdoctoral research fellowship.

CRediT Authorship Contribution Statement

All authors contributed equally to the conception, experimental work, data analysis, and preparation of the manuscript. All authors have read and approved the final version of the manuscript.

CONFLICT OF INTEREST

The authors declare that they have no known competing financial interests or personal relationships that could have influenced the work reported in this paper.

REFERENCES

Abreu, S. T., Gelves, L. G. V., Barreiro, E. J., & Lima, L. M. (2024). Revisiting nitroaromatic drugs: mechanisms of bioactivation, metabolism and toxicity and methods to synthesize nitroaromatic fragments. Journal of the Brazilian Chemical Society, 35(10), e-20240071.

Agarwal, A., Singh, V., Maurya, A., Kumar, S., & Joshi, G. (2025). Design, synthesis, and antimicrobial evaluation of new triazole-tethered tetrazole hybrids via DNA gyrase inhibition. Scientific Reports, 15(1), 34695.

Ahmad, R., Li, M., & Tong, Y. (2026). Emergence, evolution, and global dissemination of antimicrobial resistance: A One Health review. Archives of Microbiology, 208(9), 447.

Ahmed, S. K., Hussein, S., Qurbani, K., Ibrahim, R. H., Fareeq, A., Mahmood, K. A., & Mohamed, M. G. (2024). Antimicrobial resistance: Impacts, challenges, and future prospects. Journal of Medicine, Surgery, and Public Health, 2, 100081.

Akinwumi, I. A., & Ambali, O. A. (2026). Exploring synergistic effects of bioactive compounds and pharmaceuticals in therapeutic applications. Journal of Holistic Integrative Pharmacy, 7(1), 102-110.

Armengol, E. S., Harmanci, M., & Laffleur, F. (2021). Current strategies to determine antifungal and antimicrobial activity of natural compounds. Microbiological research, 252, 126867.

Bhatia, S., Biharee, A., Mondal, S., Kulkarni, S., Kumar, R., & Thareja, S. (2025). Mechanistic analysis of diverse click reactions along with their applications. European Journal of Medicinal Chemistry, 296, 117800.

Bonandi, E., Christodoulou, M. S., Fumagalli, G., Perdicchia, D., Rastelli, G., & Passarella, D. (2017). The 1, 2, 3-triazole ring as a bioisostere in medicinal chemistry. Drug Discovery Today, 22(10), 1572-1581.

Bozorov, K., Zhao, J., & Aisa, H. A. (2019). 1, 2, 3-Triazole-containing hybrids as leads in medicinal chemistry: A recent overview. Bioorganic & medicinal chemistry, 27(16), 3511-3531.

Campana, F., Lanari, D., & Vaccaro, L. (2026). Clicking the sustainability: Nobel-awarded copper catalysed azide-alkyne cycloadditions (CuAAC) through Life Cycle Assessments analysis. Green Chemistry, 28(25), 10459-10471.

Dar, B. A., Bhat, A. R., Ahmed, S., Sheikh, F. A., Jamalis, J., Kawsar, S. M., Sheikh, S. A., Patil, R. C., & Abu-Rayyan, A. (2025). Pharmacological potential and in silico studies of triazole derivatives: A comprehensive review. In Silico Research in Biomedicine, 100094.

Dixit, D., Verma, P. K., & Marwaha, R. K. (2021). A review on 'triazoles': Their chemistry, synthesis and pharmacological potentials. Journal of the Iranian Chemical Society, 18(10), 2535-2565.

El Malah, T., Abdel Mageid, R. E., Awad, H. M., & Nour, H. F. (2020). Copper (i)-catalysed azide–alkyne cycloaddition and antiproliferative activity of mono-and bis-1, 2, 3-triazole derivatives. New Journal of Chemistry, 44(42), 18256-18263.

George, N., Singh, G., Singh, R., Singh, G., Singh, H., Kaur, G., & Singh, J. (2023a). Click modified bis-appended Schiff base 1, 2, 3-triazole chemosensor for detection of Pb (II) ion and computational studies. Journal of Molecular Structure, 1288, 135666.

George, N., Singh, G., Singh, R., Singh, G., Singh, H., Kaur, G., & Singh, J. (2023b). Schiff base functionalized 1, 2, 3-triazole derivative for Fe (III) ion recognition, as N, O, O-Fe-O, O, N sandwich complex: DFT analysis. Polyhedron, 242, 116496.

Gow, N. A. (2025). Fungal cell wall biogenesis: structural complexity, regulation and inhibition. Fungal Genetics and Biology, 179, 103991.

Grady, E. N., MacDonald, J., Liu, L., Richman, A., & Yuan, Z.-C. (2016). Current knowledge and perspectives of Paenibacillus: a review. Microbial cell factories, 15(1), 203.

Ibisanmi, T. A., Jiang, X., Willcox, M., & Kumar, N. (2026). Recent advances in computational antimicrobial peptide discovery through big data, modeling, and artificial intelligence and their interplay in ushering the next golden era of drug development. Frontiers in Bioinformatics, 6, 1749404.

Jaber, A., Bitar, L., & Jaber, A. (2025). The role of nitro groups in pharmaceuticals: Effects and interactions with biological systems. Artic. Afr. J. Pharm. Sci, 5, 1-7.

Kaur, J., Saxena, M., & Rishi, N. (2021). An overview of recent advances in biomedical applications of click chemistry. Bioconjugate chemistry, 32(8), 1455-1471.

Kukov, D., Dronov, A., Frolova, M., Afanasyeva, I., & Chernykh, I. (2025). Prospects for Using 1, 2, 3-Triazole Derivatives in Medicinal Chemistry. Pharmaceutical Chemistry Journal, 59(3), 285-295.

Lengerli, D., Ibis, K., Nural, Y., & Banoglu, E. (2022). The 1, 2, 3-triazole 'all-in-one'ring system in drug discovery: A good bioisostere, a good pharmacophore, a good linker, and a versatile synthetic tool. Expert Opinion on Drug Discovery, 17(11), 1209-1236.

Lionetti, D., Day, V. W., & Blakemore, J. D. (2017). Noncovalent immobilization and surface characterization of lanthanide complexes on carbon electrodes. Dalton Transactions, 46(35), 11779-11789.

Lu, X., Zhou, J., Ming, Y., Wang, Y., He, R., Li, Y., Feng, L., Zeng, B., Du, Y., & Wang, C. (2025). Next-generation antifungal drugs: Mechanisms, efficacy, and clinical prospects. Acta Pharmaceutica Sinica B.

Lucero-Prisno III, D. E., Okesanya, O. J., Agboola, A. O., Adebayo, U. O., Adigun, O. A., Ahmed, M. M., Olaleke, N. O., Oso, T. A., Tan, M. I. R. S., & Ogaya, J. B. (2025). Emerging technologies and innovative approaches to combat antimicrobial resistance: A narrative review of next-generation therapeutic strategies. Next Bioengineering, 1, 100003.

Majumder, S., & Panigrahi, G. K. (2025). Advancements in contemporary pharmacological innovation: mechanistic insights and emerging trends in drug discovery and development. Intelligent Pharmacy, 3(2), 118-126.

Martis, G. J., Maiya, S., & Gaonkar, S. L. (2025). Synthetic Developments and Biological Insights of 1, 2, 3-Triazoles: Unravelling Scope for Drug Discovery. European Journal of Medicinal Chemistry Reports, 100315.

Oprea, I., & Smith, T. K. (2024). Click chemistry methodology: the novel paintbrush of drug design. ACS Chemical Biology, 20(1), 19-32.

Pal, R., Chakraborty, J., Mukhopadhyay, T. K., Kanungo, A., Saha, R., Chakraborty, A., Patra, D., Datta, A., & Dutta, S. (2022). Substituent effect of benzyl moiety in nitroquinoxaline small molecules upon DNA binding: cumulative destacking of DNA nucleobases leading to histone eviction. European Journal of Medicinal Chemistry, 229, 113995.

Şahin, İ. (2022). Synthesis And Characterization Of Schiff Bases Containing 1, 2, 3-Triazole Unit: Photophysical And Acetyl Choline (Ache) Inhibitory Properties. Journal of Structural Chemistry, 63(11), 1787-1796.

Salma, U., Alam, M. Z., Ahmad, S., Mohasin, M., & Khan, S. A. (2025). A comprehensive review on recent advances of remarkable scaffold Triazole based schiff base: synthesis and photoresponsive chemosensors for Al3+ ion detection. Journal of Fluorescence, 35(10), 9531-9551.

Sharma, A., Dubey, R., Bhupal, R., Patel, P., Verma, S. K., Kaya, S., & Asati, V. (2023). An insight on medicinal attributes of 1, 2, 3-and 1, 2, 4-triazole derivatives as alpha-amylase and alpha-glucosidase inhibitors. Molecular Diversity, 1-30.

Singh, G., Majeed, A., Singh, R., George, N., Singh, G., Gupta, S., Singh, H., Kaur, G., & Singh, J. (2023). CuAAC ensembled 1, 2, 3-triazole linked nanogels for targeted drug delivery: A review. RSC advances, 13(5), 2912-2936.

Singh, G., Priyanka, Sushma, Diksha, Mohit, Suman, Kaur, J. D., Saini, A., & Satija, P. (2021). Design, synthesis and photophysical aspects of 1, 2, 3-triazole appended Schiff base functionalized silanes and silatranes. New Journal of Chemistry, 45(37), 17356-17365.

Teixeira, M. M., Carvalho, D. T., Sousa, E., & Pinto, E. (2022). New antifungal agents with azole moieties. Pharmaceuticals, 15(11), 1427.

Tiwari, V. K., Jaiswal, M. K., Rajkhowa, S., & Singh, S. K. (2024). CuAAC 'Click Chemistry'-Mediated Synthesis of 1, 4-Disubstituted 1, 2, 3-Triazoles. In Click Chemistry (pp. 43-81). Springer.

Urbin, S. S., Casey, H., Price, A. P., LaBauve, A. E., & Fisher, C. L. (2025). Novel Disk diffusion Assay for Filamentous Fungi Susceptibility to antifungals (DAFFS). Journal of Microbiological Methods, 235, 107145.

Vaishnani, M. J., Bijani, S., Rahamathulla, M., Baldaniya, L., Jain, V., Thajudeen, K. Y., Ahmed, M. M., Farhana, S. A., & Pasha, I. (2024). Biological importance and synthesis of 1, 2, 3-triazole derivatives: a review. Green Chemistry Letters and Reviews, 17(1), 2307989.

Vala, D. P., Parmar, M. P., & Patel, H. M. (2026). Electrochemically driven azide–alkyne cycloaddition (E-CuAAC) via anodic oxidation using dual copper electrodes. Green Chemistry, 28(6), 2724-2735.

Wiegand, I., Hilpert, K., & Hancock, R. E. (2008). Agar and broth dilution methods to determine the minimal inhibitory concentration (MIC) of antimicrobial substances. Nature protocols, 3(2), 163-175.

APPENDIX

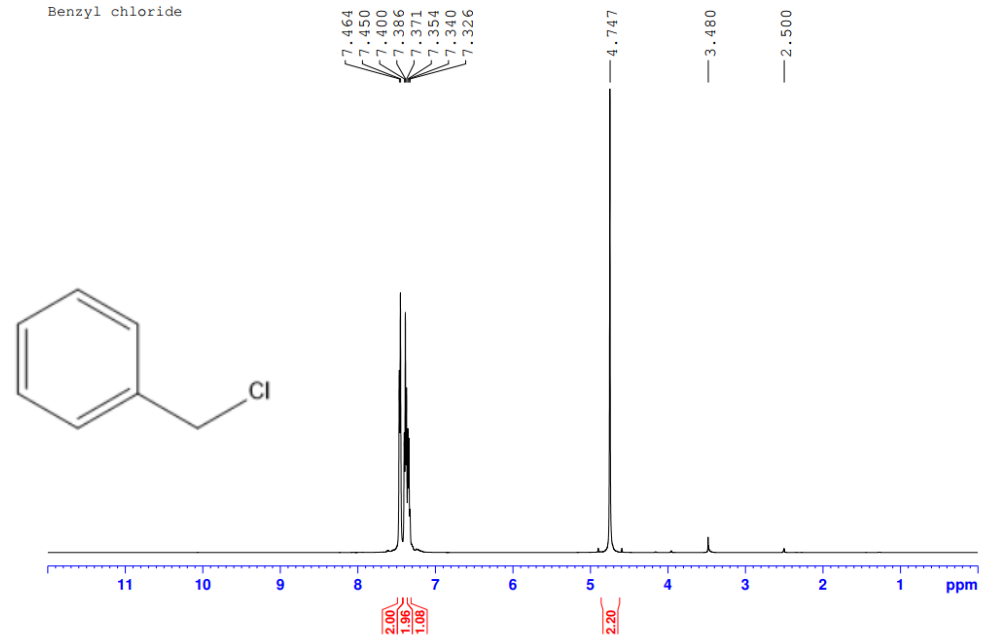

Figure S1: ^{1}H NMR Spectrum of Benzyl Chloride, Used as the Precursor for the Synthesis of (azidomethyl)benzene, Recorded at 500 MHz in DMSO-d_6 at Room Temperature. The Spectrum Displays Four Sets of Resonances Corresponding to Seven Protons, Comprising Five Aromatic Protons and Two Methylene Protons

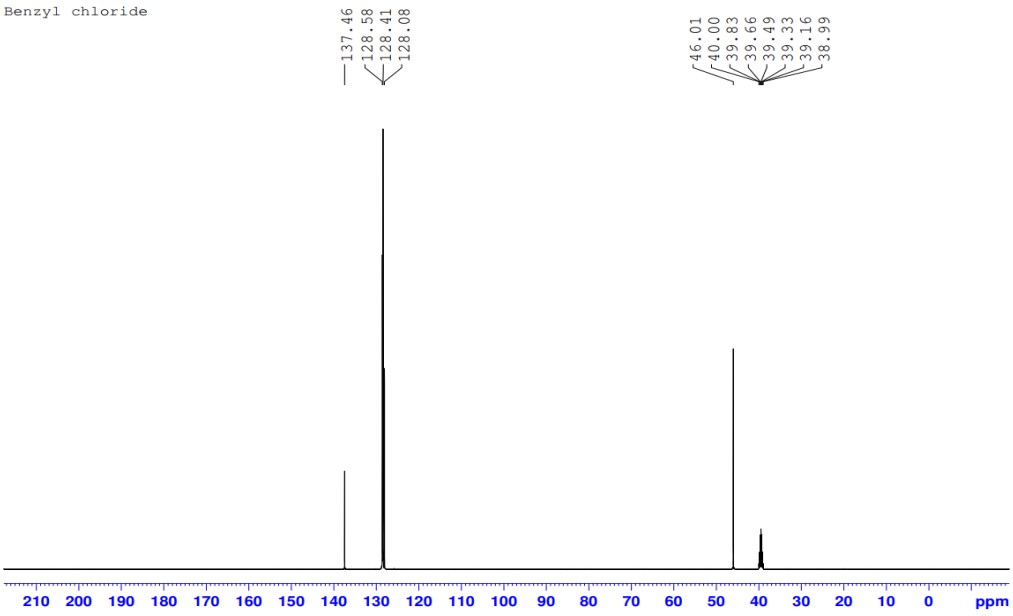

Figure S2: ^{13}C NMR Spectrum of Benzyl Chloride, Recorded at 125 MHz in DMSO-d_6 at Room Temperature. The Spectrum Exhibits Five Distinct Carbon Resonances at δ 137.46, 128.58, 128.41, 128.08, and 46.01 ppm, Corresponding to the ipso, ortho, meta, para-aromatic carbons, and the Benzylic Methylene Carbon, Respectively. The Signals Observed Between δ 38 and 40 ppm Arise from the DMSO-d_6 Solvent

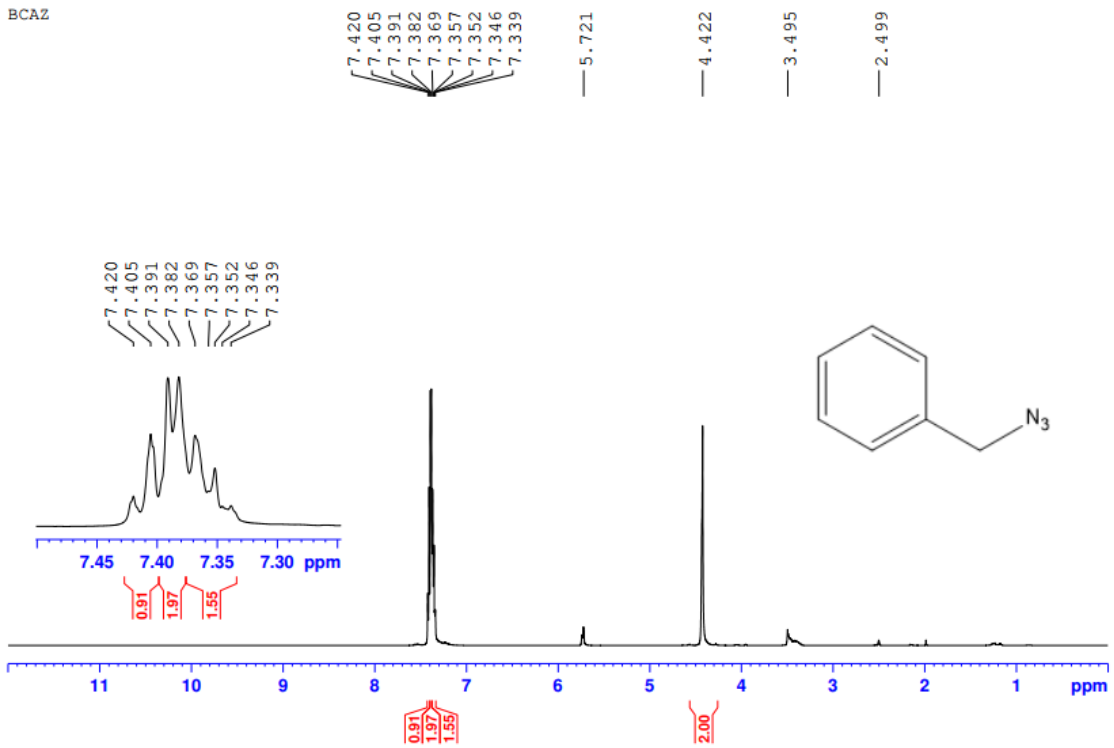

Figure S3: [1]H NMR Spectrum of (Azidomethyl)Benzene Recorded at 500 MHz in DMSO-d_6 at Room Temperature. The Spectrum Displays four Distinct Sets of Resonances Attributable to Five Aromatic Protons and Two Benzylic Methylene protons. Relative to benzyl chloride, the benzylic CH_2 Resonance is Shifted Upfield from δ 4.74 to 4.42 ppm because of Replacing the Chlorine atom with an azide (N_3) group. Minor Changes in the Aromatic Proton Resonances (δ 7.46–7.32 to 7.42–7.33 ppm) Further Support the Successful Conversion of benzyl chloride to (azidomethyl)benzene

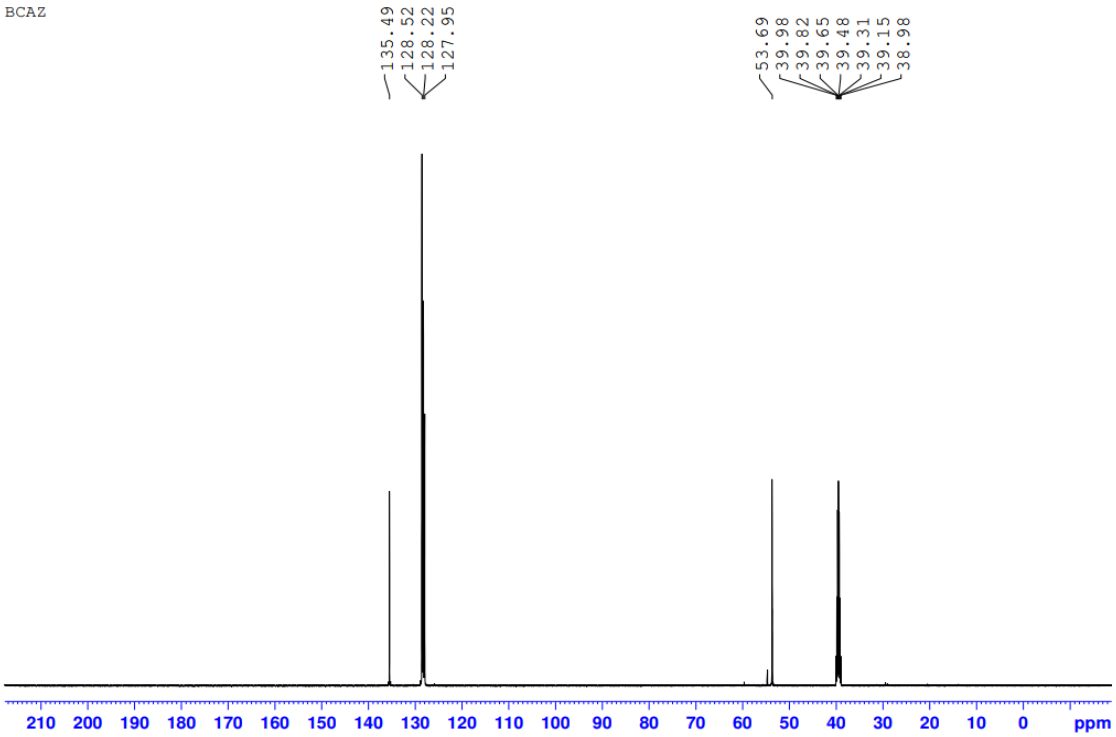

Figure S4: [13]C NMR Spectrum of (azidomethyl)benzene recorded at 125 MHz in DMSO-d_6 at room temperature. The spectrum Displays Five Distinct Carbon Resonances at δ 135.49, 128.52, 128.22, 127.95, and 53.69 ppm, Corresponding to the ipso, ortho, meta, para-aromatic carbons, and the benzylic methylene carbon, Respectively. Relative to benzyl chloride, the benzylic methylene carbon Resonance Undergoes a Downfield Shift from δ 46.01 to 53.69 ppm, Reflecting the Electronic Effect Associated with Replacement of the chlorine atom by the azide (N_3) group. Minor Changes in the Aromatic Carbon Resonances are also Observed, Further Supporting the Successful Synthesis of (azidomethyl)benzene

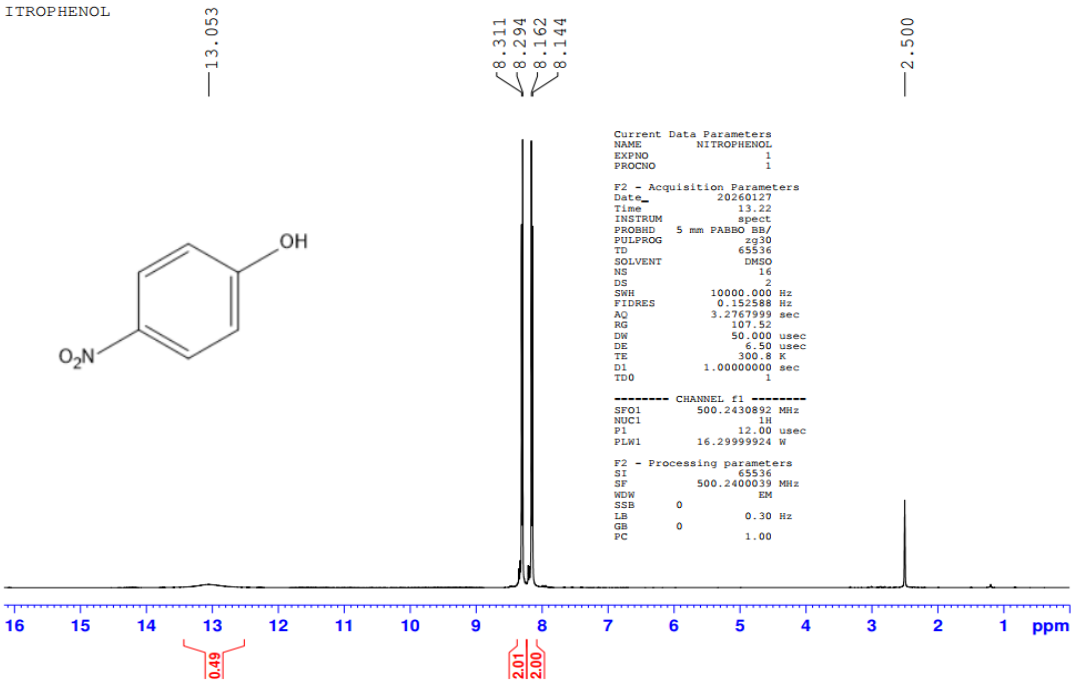

Figure S5: ^{1}H NMR Spectrum of 4-nitrophenol, used as the Precursor for the Synthesis of 1-nitro-4-(prop-2-yn-1-yloxy)benzene, Recorded at 500 MHz in DMSO-d_6 at Room Temperature. The spectrum Displays Three Distinct Sets of Resonances Corresponding to Five Protons, Comprising Four Aromatic Protons and one hydroxyl Proton

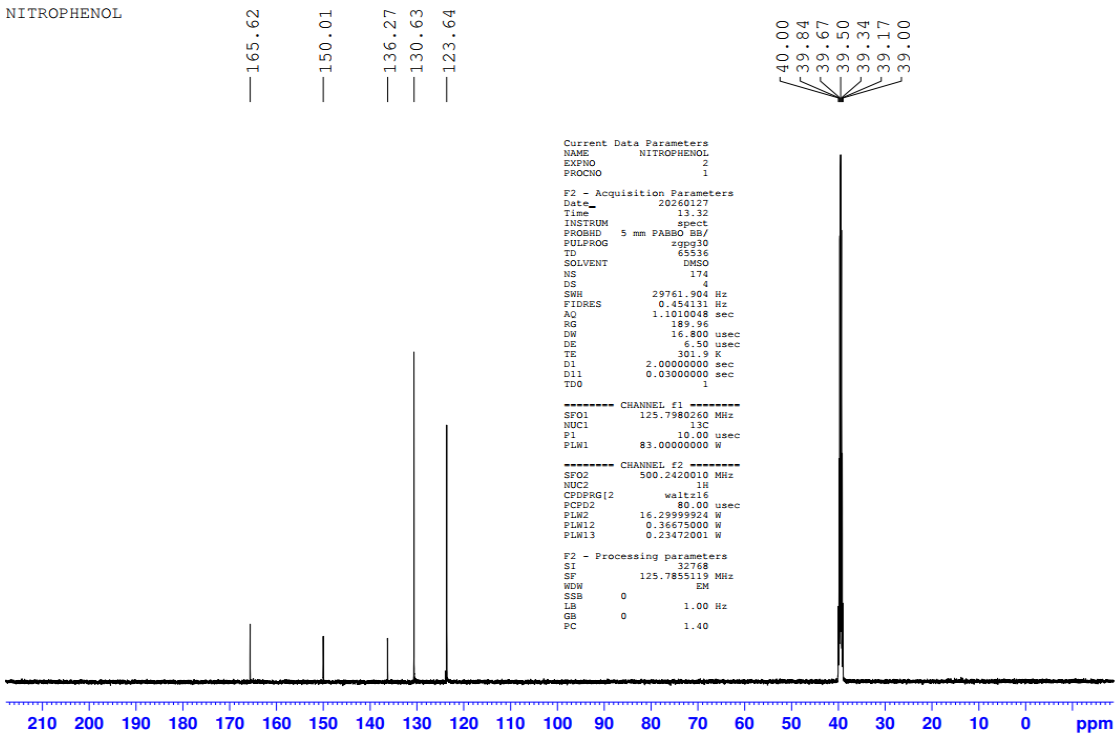

Figure S6: ^{13}C NMR Spectrum of 4-nitrophenol, used as the Precursor for the Synthesis of 1-nitro-4-(prop-2-yn-1-yloxy)benzene, Recorded at 125 MHz in DMSO-d_6 at Room Temperature. The Spectrum Exhibits Resonances at δ 165.62, 150.01, 136.27, 130.63, and 123.64 ppm, Corresponding to the Aromatic Carbon Environments of 4-nitrophenol. The Resonances at δ 165.62 and 150.01 ppm are Assigned to the Quaternary Carbons Bonded to the Hydroxyl and nitro Substituents, Respectively, while the Remaining Signals Arise from the Aromatic CH carbons. The Signals Observed between δ 39 and 40 ppm Originate from the DMSO-d_6 solvent

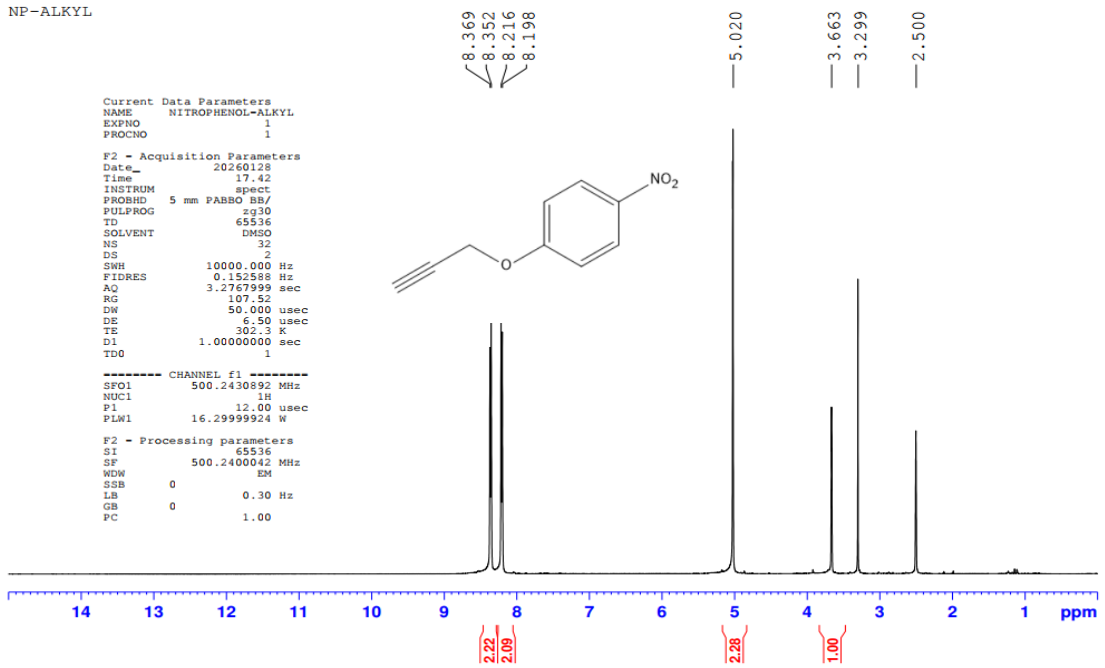

Figure S7: ^{1}H NMR Spectrum of 1-nitro-4-(prop-2-yn-1-yloxy)benzene Recorded at 500 MHz in DMSO-d_6 at Room Temperature. The Spectrum Displays Resonances Corresponding to the Aromatic Protons and the Propargyl Substituent. Compared with the Precursor (4-nitrophenol), the phenolic hydroxyl Proton Resonance is Absent, while new Signals Assigned to the propargylic methylene (OCH_2, δ 5.02 ppm) and Terminal alkyne proton (≡CH, δ 3.66 ppm) are Observed, Confirming Successful O-propargylation of the phenolic hydroxyl Group

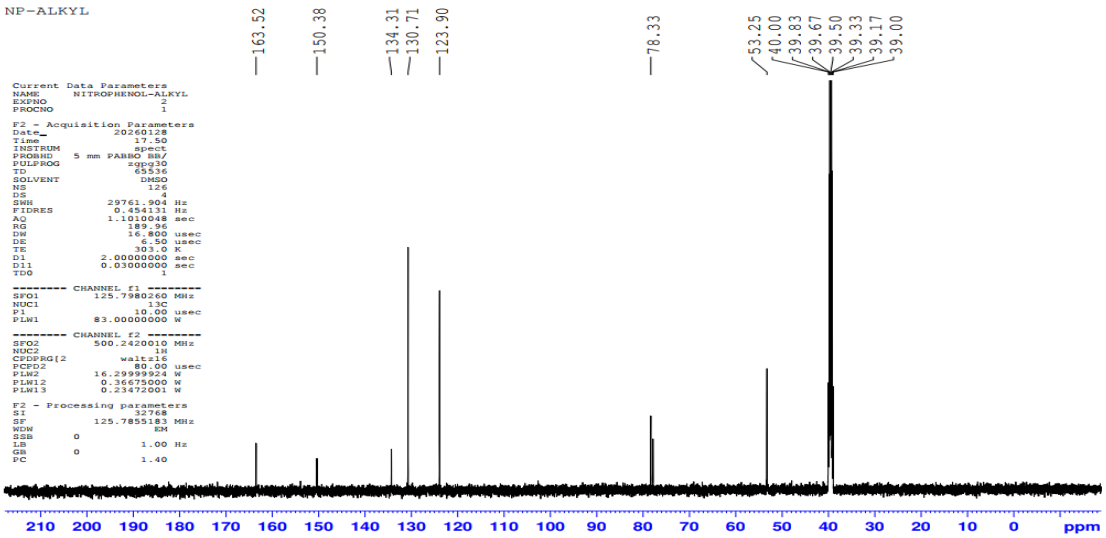

Figure S8: ^{13}C NMR Spectrum of 1-nitro-4-(prop-2-yn-1-yloxy)benzene Recorded at 125 MHz in DMSO-d_6 at Room Temperature. The Spectrum Exhibits Resonances at δ 163.52, 150.38, 134.31, 130.71, 123.90, 78.33, and 53.25 ppm, Corresponding to the Aromatic and propargyl Carbon Atoms of the Molecule. Compared with the Precursor (4-nitrophenol), the Appearance of new Resonances at δ 78.33 and 53.25 ppm, Assigned to the Acetylenic Carbon and Propargylic methylene carbon (OCH_2), Respectively, Confirms Successful O-propargylation